Recent developments with the Visible Nulling Coronagraph

Brian A. Hicks[*a,b], Richard G. Lyon[b], Matthew R. Bolcar[b], Mark Clampin[b], Peter Petrone III[c], Michael A. Helmbrecht[d], and Joseph M. Howard[b], Ian J. Miller[e]

[a]CRESST/University of Maryland, College Park, MD, USA
[b]NASA Goddard Space Flight Center, Greenbelt, MD, USA;
[c]Sigma Space Corporation, Lanham, MD, USA;
[d]Iris AO, Inc., Berkeley, CA, USA;
[e]LightMachinery, Inc., Ottawa, ON, Canada

ABSTRACT

A wide array of general astrophysics studies including detecting and characterizing habitable exoplanets could be enabled by a future large segmented telescope with sensitivity in the UV, optical, and infrared bands. When paired with a starshade or coronagraph, such an observatory could enable direct imaging and detailed spectroscopic observations of nearby Earth-like habitable zone planets. Over the past several years, a laboratory-based Visible Nulling Coronagraph (VNC) has evolved to reach requisite contrasts over a ~ 1 nm bandwidth at narrow source angle separation using a segmented deformable mirror in one arm of a Mach-Zehnder layout. More recent efforts targeted broadband performance following the addition of two sets of half-wave Fresnel rhomb achromatic phase shifters (APS) with the goal of reaching 10^{-9} contrast, at a separation of $2\lambda/D$, using a 40 nm (6%) bandwdith single mode fiber source. Here we present updates on the VNC broadband nulling effort, including approaches to addressing system contrast limitations.

Keywords: Exoplanets, high-contrast imaging, nulling coronagraphy, laboratory demonstrations, space telescopes

1. INTRODUCTION

Observations of exoplanet transits made by Kepler have provided statistics to inform future exoplanet discovery and scientific yield calculations for imminent and planned missions including TESS, JWST, and WFIRST. The combined data product of these missions will be used to refine future Earth-like exoplanet detection and characterization capabilities envisioned for the Habitable Exoplanet Imager (HabEx) and large ultraviolet, optical, infrared (LUVOIR) telescope.[1] Detecting and characterizing Earth-like habitable zone (HZ) exoplanets around nearby stars will require starlight suppression and planet light transmission at 10^{-10} contrast with 10^{-11} stability, and it has been suggested that this capability be achievable at an inner working angle (IWA) of 41 millicarcseconds at $\lambda = 1$ µm.[2] Several efforts are underway to develop and demonstrate the starshade and coronagraph technologies needed to increment towards and enable this next generation high contrast imaging science capability. Among the range of approaches under active development, the Visible Nulling Coronagraph (VNC) is a strong candidate for an internal coronagraph capable of operating with monolithic, segmented, or sparse/dilute aperture telescopes.

Experimental demonstrations of astronomical nulling interferometers (nullers) over the past 15 years[3–5] have demonstrated increasingly greater promise as an approach to direct imaging and spectroscopic study of exoplanetary systems, including spatial, size, and compositional distributions of primordial to evolved systems of exozodiacal dust and debris, and exoplanets. Nullers destructively interfere starlight to reveal the surrounding environment including dust, debris, and planets that reflect and scatter incident light from the star, as well as re-radiate absorbed light in the form of thermal blackbody emission. Interference is achieved by combining two or more beams received by multiple apertures or by splitting and recombining one or more times the light collected by a single aperture. The ideal nulling condition is satisfied when the coherent sum of interfering beams is identically zero independent of wavelength or polarization. In practice this places stringent symmetry requirements

*bahicksmail@gmail.com

Optical and Infrared Interferometry and Imaging V, edited by Fabien Malbet, Michelle J. Creech-Eakman, Peter G. Tuthill, Proc. of SPIE Vol. 9907, 99072O
 · doi: 10.1117/12.2234315

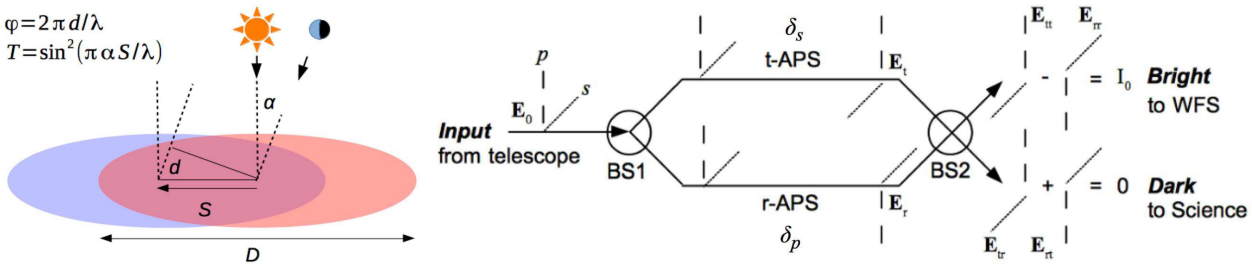

Figure 1. The object of nulling coronagraphy is to destructively interfere on-axis starlight while transmitting off-axis light at some angle α. The left panel shows off-axis phase delay between a single aperture telescope of diameter D that is interfered with a copy of itself sheared by a length S. The interferometric transmission profile T is a function of the phase difference between interfering beams, ϕ, which is a function of optical path difference, $d = S \sin\alpha \approx S\alpha$, and wavelength, λ. The right panel shows an approach to on-axis broadband electric field nulling that uses achromatic phase shifters (APS) inside of the interferometer cavity (bounded by beamsplitters BS1 and BS2) to impart retardance, δ, to orthogonal polarization components denoted s and p of the electric field, E. Subscripts r and t denote reflection and transmission following beamplitter traversals.

on interfering beams; deviation from symmetry introduces null *leakage*, for which wavefront correctors are used to compensate and improve performance. A typical design goal for a nuller is to derive wavefront symmetry requirements such that the corresponding leakage terms[6,7] do not exceed the fundamental leakage of stellar disk sizes on the order of $\sim 0.1 - 1.0$ mas diameter. These stellar sizes account for all but the few nearest and/or largest stars in the sample of A, F, G, K stars out to 30 pc whose habitable zones will be accessible with a future large ($\sim$ 10-m) space telescope.

Basic concepts pertaining to single aperture interferometric nulling coronagraphy are shown in Fig. 1. The geometry producing a periodic transmission profile (with a null at the center) is shown in the left panel, and the right panel illustrates an approach to achieving a symmetric electric field cancellation (nulling) condition, which is described in more detail below. Copies of the telescope pupil are sheared by optics inside of the nuller such that different points in the pupil overlap. For on-axis light (from the star), the phase is constant across the pupil, and therefore everywhere between interfering beams, and the condition for ideal broadband on-axis nulling is satisfied, i.e., path lengths are matched and the complex transmittance of each beam is balanced such that field vectors add in equal strength but opposite polarity. For two beam interference with a single shear as shown, the on-sky tranmission is given by $T = \sin^2(\pi\alpha S/\lambda)$, where α is the off-axis angle, S is the shear length, and λ is wavelength. Achieving transmission at smaller off-axis angles is accomplished by either working at a shorter wavelength, or by increasing shear, or both. Whereas working at a shorter wavelength requires higher precision and more stable wavefront control to reach and maintain a given contrast, increasing shear reduces the overlap region, i.e. the effective aperture, which reduces throughput and produces a larger diffraction spot.

While achieving off-axis transmission is a relatively straightforward matter of geometrical design, achieving broadband performance remains a challenge not just for nulling interferometry, but for many coronagraphic techniques. For the nuller, the challenge lies in making the symmetric output of the interferometer destructive over a broad bandpass, where "symmetric" refers to the recombined output consisting of beams that have undergone an equal numbers of beamspitter reflections and transmissions (denoted "r" and "t" in Fig. 1), and therefore have balanced amplitudes. Achromatic phase shifters (APS) are used to introduce a broadband π radian phase shift ($\lambda/2$ wave) between the symmetric output beams ("rt" and "tr") to achieve starlight cancellation, moving the starlight to the asymmetric "bright" output that combines beams of unequal reflections and transmissions ("rr" and "tt"). A description of the principle of operation of polarization-based nulling is shown in the right panel of Fig. 1 and presented in a recent work and references therein.[7]

Once broadband operation has been demonstrated with the VNC, forthcoming challenges to address include demonstrating off-axis transmission and quantifying suppression of on-axis sources with non-zero angular size. For the latter with future large telescopes, either a new approach must be realized[8] or a dual shearing nuller as shown in Fig. 2 will be needed to null the extened disk. In the left panel of this figure, a single telescope beam serves as the input for a first nuller, and the destructive output of this nuller serves as the input for a second

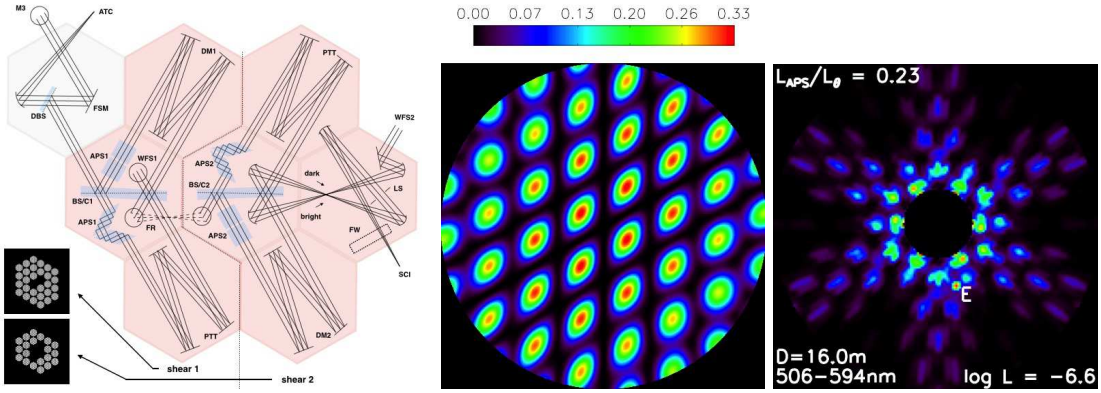

Figure 2. Coronagraphic response of θ^4 is needed for large apertures to mitigate leakage attributed to pointing jitter and finite stellar angular diameters. High-order suppression can be achieved through four beam interference using two nullers in series as shown in the schematic on the left. Interfering beams are sheared to produce the above left transmission pattern and above right stretched point spread function. Single segment shears (corresponding to D/7 for a 3-ring hexagonal array) at 60° minimize stellar leakage and maximize throughput.

nuller. Each nuller uses a beamsplitter (BS) to split the light into two paths (also referred to as "arms") and fold mirrors are used to laterally shear the two beams (not shown) while maintaining zero optical path difference. Each nuller is shown to contain sets of orthogonally-oriented Fresnel rhomb APS needed for broadband nulling. The inset of the layout shows the resultant single and dual shearing aperture functions formed by the union of 3-ring and 18-ring hexagonal arrays of mirrors, which represent a segmented telescope primary and the coronagraph deformable mirror needed for higher order wavefront control, respectively. The central panel Fig. 2 shows the resulting on-sky transmission pattern for a 20% bandpass corresponding to dual shearing in two directions by a shear length corresponding to one primary segment. The transmission scale includes the effective aperture, reflections, AR coatings, and BS efficiency. The right panel shows a simulated log scale image of a hypothetical Earth twin observed at 10 pc with the leakage dominated by the finite angular extent of the Sun-twin star.

Work to develop and demonstrate the VNC for science operations has been an ongoing effort at NASA Goddard Space Flight Center for over a decade. In the following we describe recent updates and ongoing modifications to the system including a new detector (Sec. 2.1), simplification and ruggedization of relay and imaging optics (Sec. 2.2), and planned work to improve broadband performance (Sec. 3.2) and resume characterization of candidate single mode fiber arrays meant to enable complex wavefront control when paired with piston-tip-tilt deformable mirrors.

2. LABORATORY DEMONSTRATION UPDATES

Several new components have been successfully integrated and tested with the VNC system as part of its second Technology Development for Exoplanet Mission (TDEM) milestone (MS#2) awarded to demonstrate 10^{-9} contrast in broadband light. The first narrowband VNC milestone (MS#1) demonstration made use of 12-bit CMOS detectors with a USB interface for both the bright ouput wavefront sensor and measuring contrast in the dark output. Since then, the dark channel detector has been upgraded to a low-noise and higher frame rate 16-bit sCMOS detector with the aim of improving contrast and reducing the time required to reach the targeted contrast. Relay and imaging optics have been redesigned to minimize element count, address instabilities, improve throughput, and make the layout more compact, all of which are meant to to improve reliability, mobility, and overall performance.

2.1 Detector performance

The VNC dark channel detector has been upgraded to improve demonstration capability. Measuring system contrast beyond detector dynamic range is described in the VNC TDEM Milestone #1 Final Report.[9] The limit to measurable contrast in a single pixel in a single frame is determined by the dynamic range of the detector and the contrast of the brightest pixel (suppression factor), C_0. Defining the dynamic range of the detector as the

ratio of 80% of the full well depth ($FW80$) to the RMS read noise (σ_r) dominated noise floor, the contrast of a single frame is given by

$$C = \frac{C_0 \sigma_r}{FW80}. \quad (1)$$

Assuming a starting suppressed PSF contrast of $\sim 10^{-3}$ and a detector with 16-bit resolution and $\sigma_r = 1$, single pixel contrast is $\sim 2 \times 10^{-8}$. Given adequate stability of the system, system contrast quickly approaches the single frame detector limit. Measuring and controlling contrast beyond this limit requires acquisition of large numbers of frames. The theoretical improvement to contrast sensitivity enabled by upgrading detectors in subsequent VNC TDEM efforts is summarized in Tab. 1. Equivalent peak PSF starting contrasts (attributed solely to residual DM surface errors) are associated with different starting pixel values (in ADU). The dynamic range determined by bit-depth and noise properties of the detectors used in Milestone #1 (MS#1) and Milestone #2 (MS#2) yield different initial contrast values, C_i, contrast values following a single realization, C_1, and final achievable contrasts, C_f. Environmental noise, thermal drifts, and control actuation errors add noise to the measurement of wavefront error, thereby both limiting the convergence rate and raising the contrast floor.

Table 1. Detector-limited (disturbance free environment, errorless actuation) contrast performance summary.

parameter	symbol	unit	MS#1	MS#2	notes
gain	g	e^-/ADU	1.0	0.5	
read noise	σ_r	e^- RMS	4.1	1.1	
dark current	$\jmath_d$	-	60 LSB/s	0.001 e^-/s	
80% full well (approx.)	$FW80$	ADU	3300	40000	
peak PSF core contrast	C_0	-	8.4×10^{-4}	8.4×10^{-4}	$\sigma_{DM} = 3$ nm equivalency
Initial contrast	C_i	-	1.24×10^{-5}	4.29×10^{-6}	at $2\lambda/D$
First realization contrast	C_1	-	2.91×10^{-8}	2.05×10^{-9}	at $2\lambda/D$
Final contrast	C_f	-	2.52×10^{-8}	8.82×10^{-11}	at $2\lambda/D$

Integration of the new VNC dark channel detector took place in 2015, including the addition of initialization, housekeeping, and readout routines as part of the control system software, addition of vacuum feedthroughs for cooling lines, frame grabber cable interfaces, and power. In order to preserve the oversampling of the PSF, dark channel imaging optics are being redesigned to accommodate an increase in pixel size of 2.2 µm to 6.5 µm, and this effort is described below.

2.2 Dark channel optics

The VNC's interferometric outputs provide a means of directly sensing and controlling higher spatial frequency wavefront errors via bright output detector feedback to control the deformable mirror. The VNC can also null to high contrast using the residual speckle in the science image. The optics that form a science image are referred to as the dark channel optics.

The dark channel aft-optics used for the VNC TDEM Milestone (MS#2) effort included three zoom lenses to relay the MMA pupil to either a Lyot mask or single mode fiber array (SFA). Two additional zoom lenses with a diverger lens in between were used to achieve the desired PSF sampling in the focal plane image. While necessary for matching pitch between the MMA and SFA, the zoom lens approach was one of several factors that proved detrimental to a timely completion of the VNC broadband demonstration. Until a candidate SFA has been identified as one that could significantly improve system performance (contrast, throughput, or both), there is no requirement to match SFA and MMA spacing. Both the SFA and Lyot mask achieve the same effect of removing the regions of non-overlap between the reference (delay) and MMA arms in the nuller. The regions of non-overlap include the segment gaps, the perimeter around the MMA outermost hexagonal ring, and five non-functioning segments.

A raytrace of the redesigned aft-optical system to be used in forthcoming VNC work is shown in the right panel of Fig. 3. The left panel shows a photo of the existing VNC after removal of the aft-optics used in MS#1 and MS#2. The updated system removes zoom lenses, extra folds, and a periscope to form a simplified relay

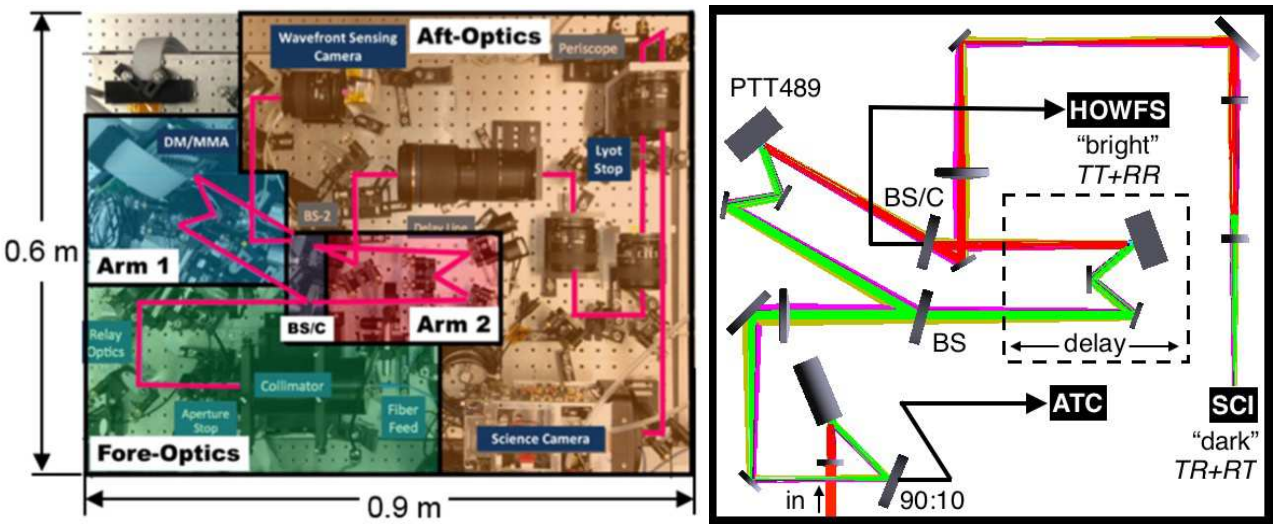

Figure 3. The VNC fits compactly on a single breadboard. Fore-optics that were used to collimate and relay a fiber-fed point source for injection into the nuller will be replaced by optics that accommodate a beam fed to the system through a vacuum window. A pick-off sends light to an angle tracker camera (ATC) that will provide feedback for a fast steering mirror (FSM) to stabilize pointing between the VNC and the external source feed. The simplified aft-optics shown in the raytrace relay the nuller outputs to the bright and dark channel cameras. A pupil is traversed each time the ray bundle changes color from predominantly red to green and vice versa.

from the dark channel output to the Lyot stop, and then to the dark channel science camera. The dark channel uses a 1:1 relay formed by achromatic doublets. A first buildup using the simplified dark channel optics has been performed and single frame captures using different bandpasses are shown in Fig. 4.

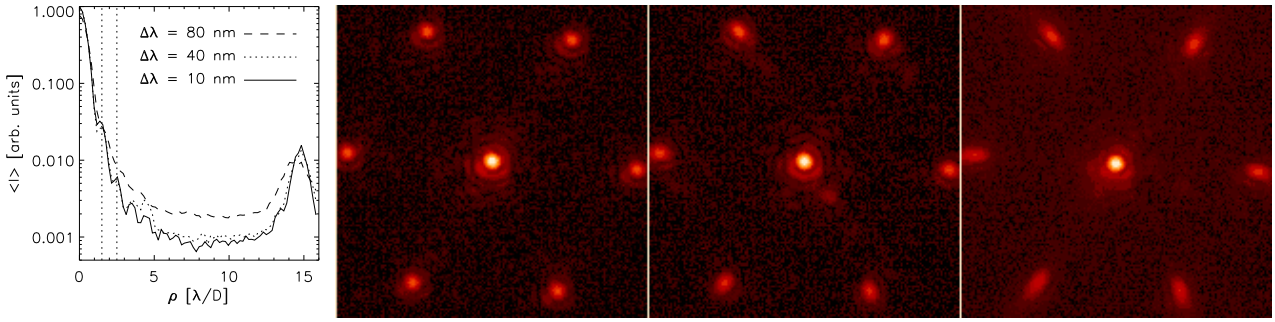

Figure 4. *Left:* azimuthally averaged radial profiles of single frame dark channel PSFs formed by the simplified dark channel optics shown in Fig. 3. *Right:* Delay arm images of a single mode fiber source traversing the delay arm of the VNC. A supercontinuum laser is paired with a filter wheel to demonstrating imaging using (*from left to right*) 10, 40, and 80 nm wide bandpasses (∼1.5%, 6%, and 12% bandwidths).

Once broadband performance is demonstrated and a SFA candidate is identified for testing, any redesign of the aft-optics needed to accommodate the SFA will be undertaken. It is noted here that modifications to the fore-optics as shown in Fig. 3 will include a fast steering mirror (FSM) and angle tracking camera (ATC) for pointing control. Preliminary work on this pointing system is described in a related work.[10]

3. ADVANCED COMPONENTS TO IMPROVE BANDPASS AND CONTRAST

In theory, APS and SFA should be capable of improving the VNC's high contrast performance to reach levels needed for detecting and characterizing Earth-like habitable zone exoplanets. While extreme precision APS may have more limited applicability, the SFA could find application in a broader range of coronagraph approaches. Work to test and increment each of these component technologies' precision is described below.

3.1 Single mode fiber array (SFA) testing

Deformable mirror yield and reliability has improved over the past decade, and even larger form factors may be expected in coming years. In addition to increasing the number of control degrees of freedom, there has also been an emphasis on the development of flatter surfaces for segmented and continuous facesheet deformable mirrors alike. Coating errors that give rise to wavefront amplitude errors, as well as residual surface errors present in deformable mirror segments and the rest of the coronagraphic optical train can be corrected by a SFA, thereby improving the wavefront quality to reach deeper contrasts and/or access to more discovery space in the high contrast image plane. Simulated filtering of higher order wavefront errors is shown in the right panel of Fig. 5, where the lowest order piston or amplitude errors are separated from the higher order terms. Ultimately, the SFA functions in concert with the MMA to actively correct amplitude errors by adjusting tip and tilt to affect the coupling overlap integral in each segment-fiber pair.

The SFA enable this complex (phase and amplitude) wavefront correction as a passive unit. The alternative approach to yielding comparable control is to use two DMs (not necessarily MMAs), one in a pupil, the other in an intermediate optical plane, leveraging the Talbot effect. As a passive component, the SFA does not require added amplifier electronics or the numerous signal leads that are needed for deformable mirrors, thereby reducing complexity and a large number of failure modes.

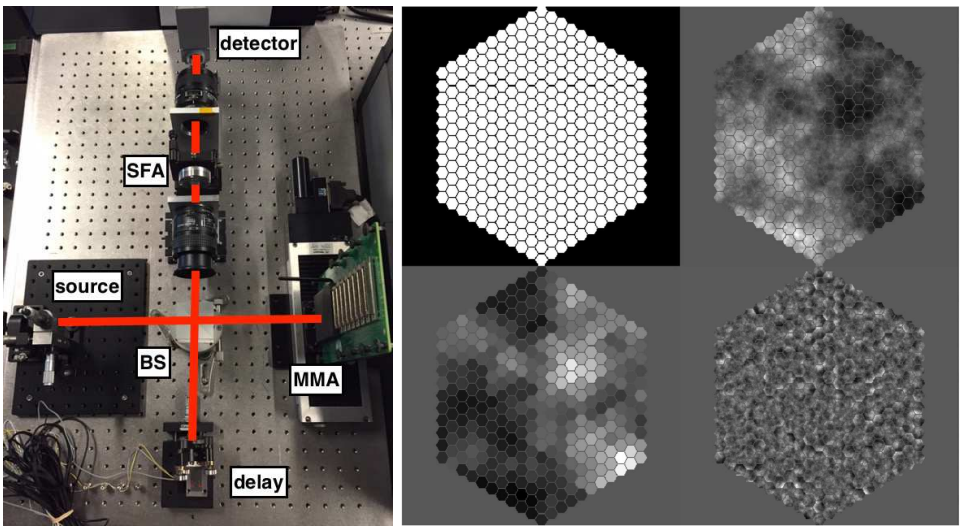

Figure 5. *Left*: components of a SFA characterization testbed that will be used to quantify transmission and dispersion properties, and potentially identify a candidate component to be incorporated for demonstrations with the VNC. Additional optics and a second detector may be added to pick off light prior to entering the SFA for simultaneously monitoring interference between the MMA and delay reference, the SFA exit pupil, as well as the imaged PSF. *Right*: Decomposition of wavefront phase or amplitude errors that are filtered by the SFA and controlled by the MMA. Proceding clockwise from the upper right, ensemble wavefront errors are filtered by the SFA, leaving residual piston and amplitude errors that are to nominally made uniform across the array.

Work to characterize and identify a candidate SFA to demonstrate in tandem with or following the next steps in VNC TDEM efforts will be begin by using the setup shown in Fig. 5. Candidate SFAs will first be characterized independent of the MMA, quantifying transmission properties including coupled throughput and dispersion. The reference surface profiles will manifest as a shift in broad band fringe packet center for each fiber in the array, which will be scanned by a mirror mounted on a delay stage. A next step will demonstrate controlled tip/tilt coupling of segments across a MMA into the SFA. After optimizing the coupling, segments in the mirror array can be independently scanned through the remaining several waves of stroke range to minimize piston wavefront error across the array, thereby optimizing the Strehl of the imaged PSF. The wavefront errors at the spatial frequency scale of one cycle per MMA segment and higher will be attenuated and show up as coupled throughput loss. An effort will be made to quantify these losses in comparison to previous independent measurements of segment surface errors that have been decomposed into an orthogonal basis.

3.2 Next generation achromatic phase shifters

In theory, it should be possible to improve Fresnel rhomb APS performance beyond what is expected from the rhombs that have recently been in use in the VNC[11] using a single layer of magnesium flouride deposited on, e.g., BK7 rhombs to reduce the RMS retardance variation over a given bandpass.[12,13] A sample design using this single layer coating approach is presented in Fig. 6.

An advantage of this design is that it can be measured with conventional thin film equipment. The coating layer can be deposited on a material with a high index of refraction, e.g., sapphire or SF11, in order to measure its thickness very accurately using ellipsometry. Once the film thickness and properties are characterized, it can be deposited on high grade (homogeneous) glass, again using a high index material as a witness to verify the deposition layer thickness.

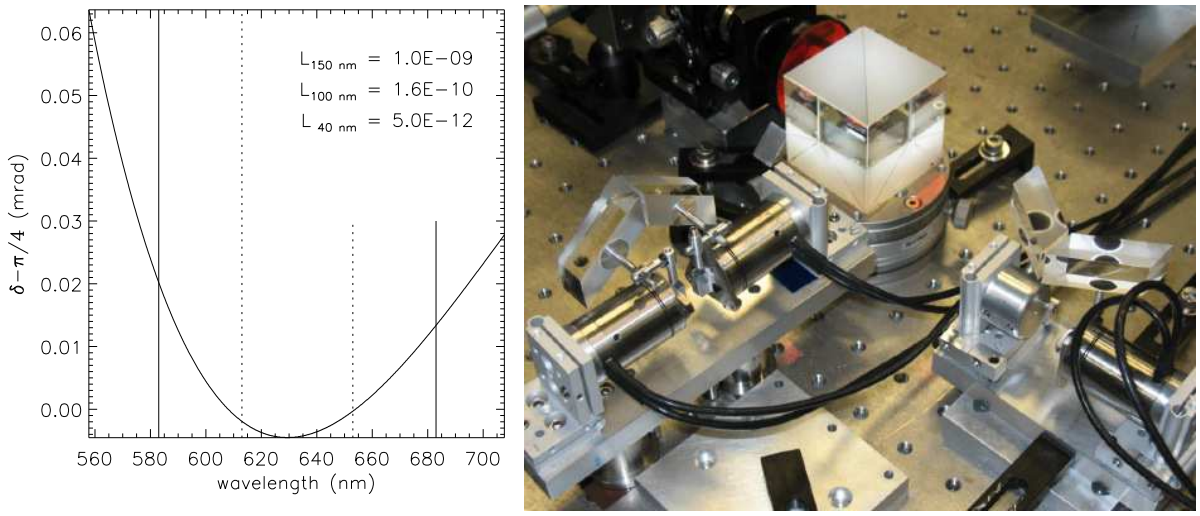

Figure 6. *Left*: a BK7 APS design using a single 12.7 nm thick MgF2 layer coated on each TIR surface using an AOI of 51.4723 degrees. Leakages are calculated for 150, 100, and 40 nm bandpasses. Note that in the presence of no other errors leakage levels represent the intensity of the suppressed PSF relative to the normalized, unsuppressed PSF. *Right*: the VNC TDEM MS#2 Fresnel rhomb engineering APS mounted in a test configuration that was built to develop and test fine positioning controls and characterize the APS independent of ongoing VNC demonstrations.

This theoretical improvement in performance effectively shifts chromatic leakage from being a top contributor to the error budget (contending with that attributed to stellar angular extent) to being almost a negligible contributor. More work needs to be done to quantify the effects of any small but significant bulk material birefringence, striae, and inclusions that can be expected to compromise APS performance.

3.3 Contrast enhancements enabled by advanced components

By refining the APS design and incorporating a successful build of these components along with a SFA into the VNC, the limits to achievable contrast should be improved. Fig. 7 compares the unsuppressed PSF (left panel) with suppressed PSFs assuming current (central panel) and enhanced component capability (right panel). Only deformable mirror residual surface errors and chromatic leakage attributed to error in retardance across the MS#2 40 nm bandpass are assumed in an otherwise perfect system. The assumed retardance errors are for uncoated APS rhombs with $\sigma_\delta = 345$ µrad RMS, and a point design coated solution yielding $\sigma_\delta = 1.17$ µrad RMS. The values for the residual DM surface errors correspond to operation without a SFA to $\sigma_{DM} = 3.0$ nm RMS, and using an SFA to filter to $\sigma_{DM} = 1.0$ nm RMS. PSFs are shown on a log scale the lowest order piston, tip, or tilt errors are corrected perfectly. Contrast statistics within superimposed wedge-shaped regions with different outer working angles are are presented in Tab. 2. Each 55° wedge has an IWA of $1.3\lambda/D$.

4. SUMMARY

The VNC uses a combination of active and passive components to work towards meeting the common goal of the high contrast imaging community: $< 10^{-9}$ contrast at $\sim 3\lambda/D$ IWA or better over a spectral bandpass of $> 10\%$. In its most simplistic form, the VNC works by destructive and constructive interference. Starlight is relayed through the system such that a central destructive interference null condition exists in the science channel and stellar photons instead appear in the bright pupil camera for wavefront control. Faint off-axis sources of interest such as exoplanets and debris disk structures that are located at constructive interference maxima are transmitted to the dark science focal plane for detection and characterization.

The VNC requires an APS that corrects the phase difference between the two arms of the nuller to π over a sufficient bandpass for future exoplanet detection and characterization, typically on the order of $\Delta\lambda/\lambda = 0.1$. Without an APS, the null is inherently narrowband due to the phase shift being set by the path length difference in the two arms of the nuller. The VNC previously achieved $< 10^{-8}$ contrast at an inner working angle (IWA) of $2\lambda/D$ through the use of a multiple mirror array (MMA). Demonstrating broadband performance at comparable or better contrast using Fresnel rhomb APS remains a near-term goal for upcoming VNC work.

Enabling technologies and control routine innovations are undergoing continual development in VNC efforts. Future TDEM work has been advanced through both IRAD, and SBIR Phase-I and II efforts. The VNC testbed has been developed at GSFC and has run in air in a closed chamber environment, and the VNT system has been readied for vacuum operation. A simplification of the aft-optical system should improve performance for the next VNC Milestone (MS#3) aimed at demonstrating sequential wavefront control with a macro-scale actively-controlled segmented mirror.[10] Ultimately meeting all TDEM Milestone goals will strengthen the case that broadband and stable visible light high contrast imaging through nulling can be achieved to realize the future missions such as LUVOIR.[14]

Table 2. Expected dark channel contrast statistics corresponding to regions shown in Fig. 7.

σ_δ	345 µrad			1.17 µrad		
σ_{DM}	3.0 nm			1.0 nm		
OWA $[\lambda/D]$	16	4.0	2.5	16	4.0	2.5
maximum	7.6^{-8}	3.4^{-8}	2.9^{-8}	1.2^{-8}	8.6^{-10}	2.9^{-10}
minimum	2.2^{-11}	1.6^{-10}	6.6^{-10}	1.5^{-12}	8.9^{-12}	2.9^{-11}
median	2.7^{-9}	3.4^{-9}	9.8^{-9}	3.5^{-10}	9.7^{-11}	2.0^{-10}
mean	5.6^{-9}	6.4^{-9}	1.2^{-8}	6.5^{-10}	1.8^{-10}	3.3^{-10}
RMS	7.3^{-9}	7.3^{-9}	8.3^{-9}	9.2^{-10}	2.0^{-10}	2.2^{-10}

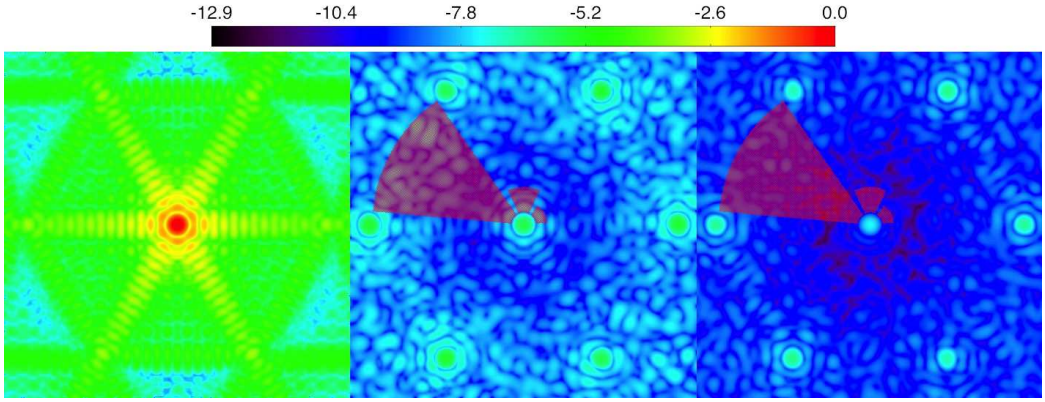

Figure 7. Log-scale normalized dark channel focal plane intensity of (*left*) the unsuppressed PSF, (*center*) the suppressed PSF with σ_δ = 345 µrad RMS per TIR and 3 nm RMS residual DM surface errors, and (*right*) the suppressed PSF assuming σ_δ = 1.17 µrad RMS per TIR and 3 nm RMS residual DM surface errors.

ACKNOWLEDGMENTS

The authors acknowledge support from NASA/Goddard Space Flight Center Internal Research and Development (IRAD), and from the NASA Strategic Astrophysics Technology (SAT) Technology Development for Exoplanet Missions (TDEM) program.

REFERENCES

[1] Thronson, H., Bolcar, M. R., Clampin, M., Crooke, J., Feinberg, L., Oegerle, W., Rioux, N., Stahl, H. P., and Stapelfeldt, K., "Path to a UV/optical/IR flagship: review of ATLAST and its predecessors," *J. Astron. Tel. Inst. & Syst..* **2**, 041210 (2016).

[2] Stark, C. C., Roberge, A., Mandell, A., Clampin, M., Domagal-Goldman, S. D., McElwain, M. W., and Stapelfeldt, K. R., "Lower Limits on Aperture Size for an ExoEarth Detecting Coronagraphic Mission," *Astrophys. J.* **808**, 149 (Aug. 2015).

[3] Wallace, K., Hardy, G., and Serabyn, E., "Deep and stable interferometric nulling of broadband light with implications for observing planets around nearby stars," *Nature* **406**, 700–702 (Aug. 2000).

[4] Gappinger, R. O., Diaz, R. T., Ksendzov, A., Lawson, P. R., Lay, O. P., Liewer, K. M., Loya, F. M., Martin, S. R., Serabyn, E., and Wallace, J. K., "Experimental evaluation of achromatic phase shifters for mid-infrared starlight suppression," *Appl. Opt.* **48**, 868–880 (Feb. 2009).

[5] Lyon, R. G., Clampin, M., Petrone, P., Mallik, U., Madison, T., and Bolcar, M. R., "High contrast vacuum nuller testbed (VNT) contrast, performance, and null control," *Proc. SPIE* **8442** (Sept. 2012).

[6] Serabyn, E., "Nulling interferometry: symmetry requirements and experimental results," *Proc. SPIE* **4006**, 328–339 (July 2000).

[7] Hicks, B. A., "Exoplanet detection and characterization via parallel broadband nulling coronagraphy," *J. Astron. Tel. Inst. & Syst..* **2**, 011015 (Jan. 2016).

[8] Lyon, R. G., Hicks, B. A., Clampin, M., and Petrone, III, P., "Phase-Occultation Nulling Coronagraphy," *ArXiv e-prints* (Apr. 2015).

[9] Clampin, M., Lyon, R., Petrone III, P., Mallik, U., Bolcar, M., Madison, T., and Helmbrecht, M., "Visible nulling coronagraph technology maturation High contrast imaging and characterization of exoplanets," tech. rep., NASA/Technology Development for Exoplanet Missions Final Report, JPL Document D-80950, https://exep.jpl.nasa.gov/technology/Clampin_Report_FINAL.pdf (2013).

[10] Hicks, B. A., Lyon, R. G., Petrone, P., Miller, I., Bolcar, M. R., Clampin, M., , Helmbrecht, M., and Mallik, U., "The Segmented Aperture Interferometric Nulling Testbed (SAINT) I: overview and air-side system description," *Proc. SPIE* **9904** (2016).

[11] Hicks, B. A., Lyon, R. G., Petrone, P., Miller, I., Bolcar, M. R., Clampin, M., , Helmbrecht, M., and Mallik, U., "Demonstrating broadband billion-to-one contrast with the Visible Nulling Coronagraph," *Proc. SPIE* **9605** (2015).

[12] King, R. J., "Quarter-wave retardation systems based on the Fresnel rhomb principle," *Journal of Scientific Instruments* **43**, 617–622 (Sept. 1966).

[13] Clapham, P. B., Downs, M. J., and King, R. J., "Some applications of thin films to polarization devices," *Appl. Opt.* **8**, 1965 (Oct. 1969).

[14] Bolcar, M. R., Balasubramanian, K., Crooke, J., Feinberg, L., Quijada, M., Rauscher, B., Redding, D., Rioux, N., Shaklan, S., Stahl, H. P., Stahle, C., and Thronson, H., "Technology gap assessment for a future large-aperture ultraviolet-optical-infrared space telescope," *J. Astron. Tel. Inst. & Syst..* **2**, 041209 (2016).